NANO · MICRO small
www.small-journal.com

Air Retention under Water by the Floating Fern *Salvinia*: The Crucial Role of a Trapped Air Layer as a Pneumatic Spring

Daniel Gandyra, Stefan Walheim, Stanislav Gorb, Petra Ditsche, Wilhelm Barthlott, and Thomas Schimmel**

The ability of floating ferns *Salvinia* to keep a permanent layer of air under water is of great interest, e.g., for drag-reducing ship coatings. The air-retaining hairs are superhydrophobic, but have hydrophilic tips at their ends, pinning the air–water interface. Here, experimental and theoretical approaches are used to examine the contribution of this pinning effect for air-layer stability under pressure changes. By applying the capillary adhesion technique, the adhesion forces of individual hairs to the water surface is determined to be about 20 µN per hair. Using confocal microscopy and fluorescence labeling, it is found that the leaves maintain a stable air layer up to an underpressure of 65 mbar. Combining both results, overall pinning forces are obtained, which account for only about 1% of the total air-retaining force. It is suggested that the restoring force of the entrapped air layer is responsible for the remaining 99%. This model of the entrapped air acting is verified as a pneumatic spring ("air-spring") by an experiment shortcircuiting the air layer, which results in immediate air loss. Thus, the plant enhances its air-layer stability against pressure fluctuations by a factor of 100 by utilizing the entrapped air volume as an elastic spring.

1. Introduction

Superhydrophobic air-retaining surfaces underwater offer a great potential for drag reduction of ship hull coatings or in fluid transportation.[1–6] Additionally, they will extend the wide range of applications of superhydrophobic surfaces in the field of water-repellence and self-cleaning[7–17] as it was recently shown by measuring the friction reduction[18–24] or the slip length of the hydrodynamic velocity profile as a corresponding quantity.[4,25–29] However, for any technical application of underwater air layers, the long-term stability (persistence) of the air layer is of vital importance.[30–34] In order to retain air, these structures have to be small and the material used should be as hydrophobic as possible. Konrad et al.[35] described a quantitative relationship between structure size, contact angle, and maximum immersion depth at which the air can still be kept stable. In a recent publication,[36,37] Xu et al. showed experimentally that a trench embossed in Teflon with a width of 150 µm can retain air at a depth of 55 cm, but not at 1 m depth. At 50 µm width, a stable air retention up to 1.5 m could be shown. So in order to create a functional surface on a large scale, it is essential to create hydrophobic structures with topography on a very small scale. With respect to these parameters most artificial surfaces developed so far failed.[20,35,38,39] Surprisingly, the floating fern *Salvinia molesta* is able to maintain a *permanent* air layer under water during its lifetime. Therefore, the surface of *Salvinia* leaves is considered as a biological model for technological air-retaining surfaces.[5,40–49] In order to have an effective air retention, the upper side of the leaves is covered with elastic, superhydrophobic, eggbeater-shaped trichomes (later called "hairs") (see **Figure 1**a,b). The backside of the leaf is hydrophilic, and therefore staying in permanent direct contact with water. The complexly shaped hairs on the top side are coated with nanoscale wax crystals, which make their surface superhydrophobic and prevent water from penetrating between the hairs. This unique structure of *Salvinia* hairs already led to the inspiration of micro-structured oil collecting materials.[50–52] Five criteria have been defined[30] to be important for air retention under water: 1) hydrophobic chemistry, 2) nanostructured topography, 3) hierarchic architecture, 4) undercut structural features (overhanging structures), and 5)

Dr. D. Gandyra, Dr. S. Walheim, Prof. T. Schimmel
Institute of Nanotechnology (INT)
Karlsruhe Institute of Technology (KIT)
Hermann-von-Helmholtz-Platz 1, Eggenstein-Leopoldshafen 76344, Germany
E-mail: stefan.walheim@kit.edu; thomas.schimmel@kit.edu
Prof. S. Gorb
Department of Functional Morphology and Biomechanics
Institute of Zoology
Kiel University
Am Botanischen Garten 1–9, Kiel 24118, Germany
Dr. P. Ditsche, Prof. W. Barthlott
Nees Institute for Biodiversity of Plants
University of Bonn
Venusbergweg 22, Bonn 53115, Germany
Prof. T. Schimmel
Institute of Applied Physics (APH) and Materials Research Center for Energy Systems (MZE)
Karlsruhe Institute of Technology (KIT)
Wolfgang-Gaede-Straße 1, Karlsruhe 76131, Germany
The ORCID identification number(s) for the author(s) of this article can be found under https://doi.org/10.1002/smll.202003425.

DOI: 10.1002/smll.202003425

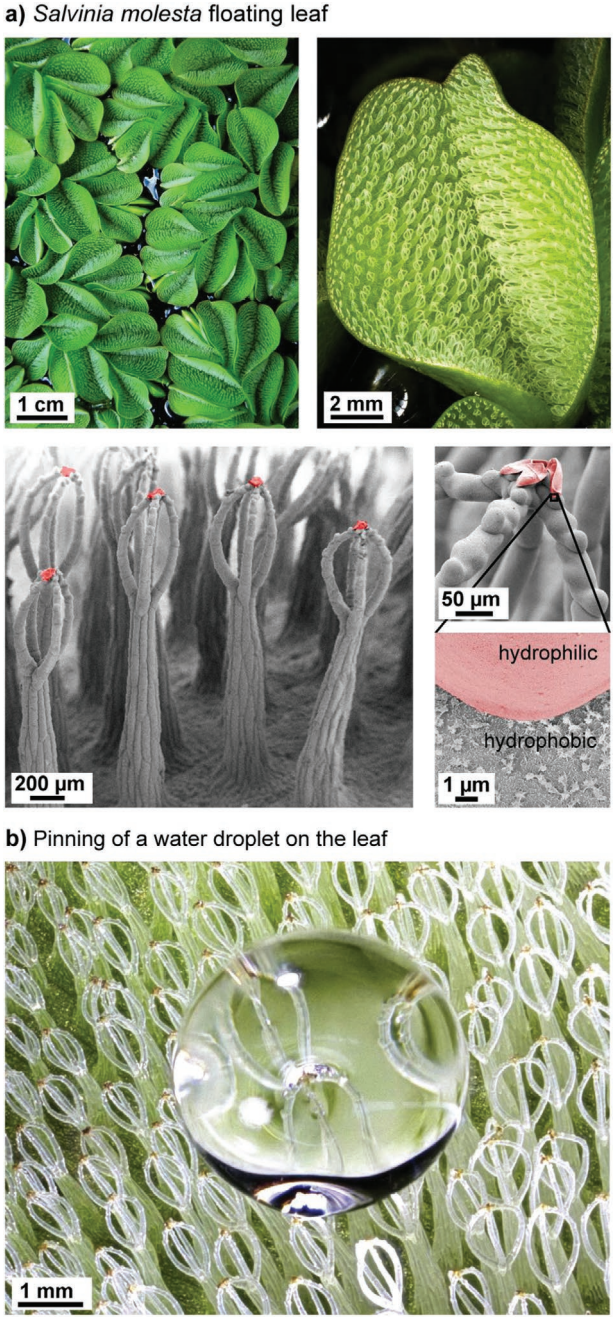

Figure 1. The floating fern *Salvinia molesta*: a) group of plants (optical image, left) and single leaf (optical image, right). The leaf surface is densely covered with superhydrophobic eggbeater-shaped hairs having hydrophilic tips at their ends (areas shown in red in the SEM images). This leads to a "pinning" of the water, e.g., in case of an attached droplet (optical image in (b)). Fully submerged in water, this pinning is one reason for the high persistence of the air layer trapped between the hairs.

the elasticity of the hairs. All these features are common for the top side of the *Salvinia* leaves and define the *Salvinia* effect.[28]

Salvinia molesta and some of its relatives feature an additional notable detail: At the tips of the eggbeater-shaped hairs, the submicron-sized wax crystals are missing, which make these areas hydrophilic and therefore adhesive to water.[53] This remarkable feature was named *Salvinia* paradox,[1] because it is in contrast to many other superhydrophobic surfaces in nature, which are entirely hydrophobic.[54] The effect of these hydrophilic anchor cells is that they are "pinning" the water and in this way stabilize the air–water interface.[1]

Moreover, the elasticity of the hairs is of great importance for the stability of the air layer under fluctuating pressure situations. These result in variations of the air layer thickness to which the eggbeater-shaped hairs can adjust either by bending or by compression and expansion.[55,56] The spring constant of the hairs of *Salvinia molesta* is 2.1 N m^{-1}. When the adjustability of the hairs reaches its limit, the pinning force of the hair tips (the so-called apex) helps to stabilize the air layer (the *Salvinia* paradox).[1] This advantageous property was already investigated in our previous publication,[1] theoretically described (see, e.g., ref. [57]) and already implemented in artificial model surfaces.[58]

Here, we raise the question how much the pinning force of the tips (*Salvinia* paradox) contributes to the stability of the air layer of the *Salvinia molesta* leaf in underpressure situations and whether this force is sufficient to quantitatively explain the pressure fluctuation stability observed experimentally.

To answer this question, we show a quantitative analysis of the pinning force of a single hair with the capillary adhesion technique[56] and present a statistical evaluation. By using the adhesion force, averaged over the surface of the leaf we can calculate a corresponding underpressure stability limit, which defines the point at which the connection of the air/water interface would break. We show that the calculated value would be around 0.6 mbar for *Salvinia molesta* leaves. In our experiment, however, we could apply a much higher underpressure without air loss. When applying an underpressure to a submerged leaf, we found a 100 times higher persistence than could be expected from this simple model calculation, assuming the hydrophilic pins alone to be responsible for keeping the air layer in an underpressure situation. This fact led us to a quantitative understanding of the ability of *Salvinia molesta* to retain a stable air layer under water: The thin layer of entrapped air serves as a pneumatic spring which provides the restoring force preventing air loss. In our experiments, the air spring was responsible for ≈99% of the total restoring force for the air layer against negative pressure, occurring, e.g., in pressure fluctuations. We determine that without the air spring in operation, the leaf loses the air already at 0.6 mbar underpressure, which is the value, corresponding to a hydrostatic pressure of a water depth of 0.6 cm. This also yields a new key parameter for the design of artificial, air retaining surfaces, using the *Salvinia* effect.

2. Results and Discussion

2.1. Measurement of Single Hair Adhesion Forces

The conclusions above were drawn based on results obtained by using our capillary adhesion technique[56] to measure the adhesion force between the tip of a single hair and a liquid (**Figure 2**). The hair was put into contact with water by its

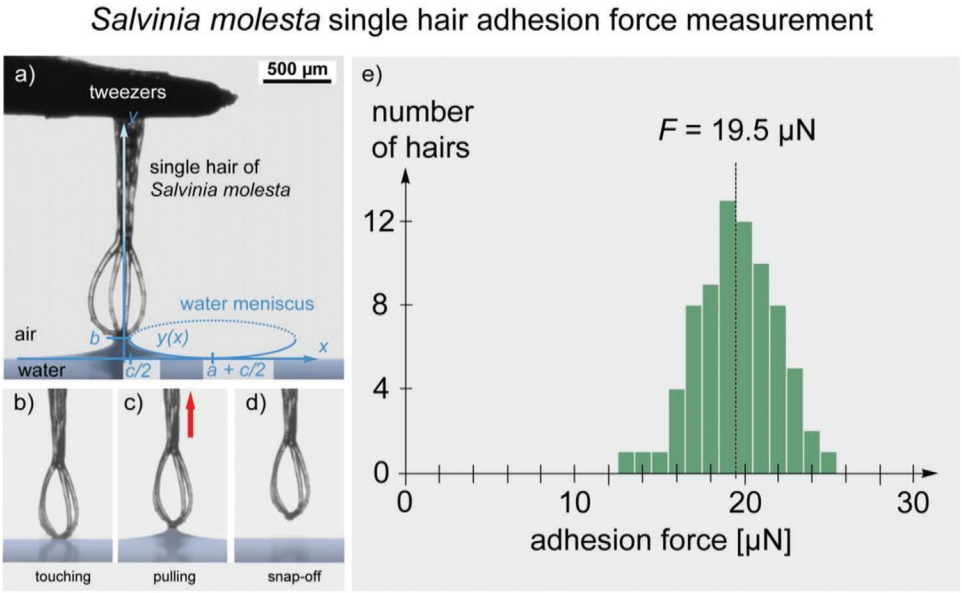

Figure 2. Single hair water adhesion force measurement: b–d) a *Salvinia molesta* hair was attached with its tip downward to a water surface and removed from it. The profile of the developing meniscus taken shortly before snap-off was fitted with an elliptic function $y(x)$ (shown in (a)). The evaluation of the meniscus surface area allows to determine the energy and force needed for its creation, which equals the water adhesion force of the hair tip. Investigating 75 individual *S. molesta* hairs resulted in the force histogram shown in (d). The average water adhesion force was 19.5 µN.

hydrophilic tip, pointing straight downward to the water surface from above and was then removed (lifted up) again. Thus, a water meniscus was created which snapped off at a certain point. This happens when the tensile force caused by the increasing meniscus exceeded the water adhesion force between the tip of the hair and the water. An analysis based on evaluations of the surface energy of the meniscus as a function of distance shortly before snap-off leads to the value of the water adhesion force as described in the Experimental Section and in more detail in our previous paper.[56] Using this technique, the investigation of the water adhesion force of the tip of a single *Salvinia molesta* hair to the water surface results in an average value of 19.5 ± 0.7 µN per hair, when averaging over many different such experiments performed with different hairs. We examined 75 individual eggbeater-shaped hairs taken from the central region of an *S. molesta* leaf, 3 mm away from the edge, 5 hairs from each of 15 different adult leaves, in order to get representative information. The distribution of single values is given in Figure 2, showing a peak around the average value of 19.5 µN. Parts of these results have been shown in our previous work.[56] Here, we show the statistical distribution of individual adhesion forces. From the water adhesion force, we calculated the expected underpressure that an individual *S. molesta* leaf can withstand, before the adhesive contact of hair tips to the water begins to break and water contact is lost. The hair density of *S. molesta* leaves, as investigated for the leaves used in our study was (3.1 ± 0.4) mm^{-2} in the middle region 3 mm away from the edge. This leads to a water adhesion force per area of (60.6 ± 9.0) µN mm^{-2}, which corresponds to an underpressure of (0.606 ± 0.090) mbar. Beyond that pressure, the hydrophilic tip can no longer keep the contact to the water, withstanding the external forces due to underpressure. Once this contact is broken, air bubbles form and the air layer is lost.

2.2. Air Layer Stability on a Submerged Leaf of *Salvinia molesta* Studied by Laser Scanning Confocal Microscope (LSCM)

To assess the air layer persistence on a submerged leaf, we measured the negative pressure needed to make the first hair tip losing its contact with the water: When exposed to an increasing underpressure, the trapped air of a leaf expands and the air–water interface between the hair tips curves upward, obtaining a more arch-like shape.[49]

We studied this process of meniscus deformation due to underpressure experimentally by using a home-made pressure cell adapted to a LSCM.[59] For studying the air-to-water interface, the interface was fluorescence labeled by staining it with fluorescing pigment particles (PS10 (radiant color)), which sedimented to the water/air interface. The emitted fluorescence signal from the interface was subsequently detected with the LSCM. When a certain underpressure value was achieved, at first one hair-tip-to-water contact was lost, followed by further snap-off events with increasing underpressure (**Figure 3**). This process was perfectly reversible and the underpressure needed for the loss of contact of the first hair serves as a measure for the air layer persistence. The experimentally observed value needed for the first snap-off was (56.8 ± 2.5) mbar, based on the investigation of 50 half leaves.

As this is (94 ± 15) times, i.e., about two orders of magnitude—more than the calculated value, the high persistence of the air layer on *Salvinia molesta* leaves cannot be explained by the attractive forces of the hydrophilic tips of the hairs and the water alone. It has to have a second component, which is able to explain the remaining almost 99% of the air retaining force—an important, but so far neglected component, that drastically increases the air layer stability of the leaves.

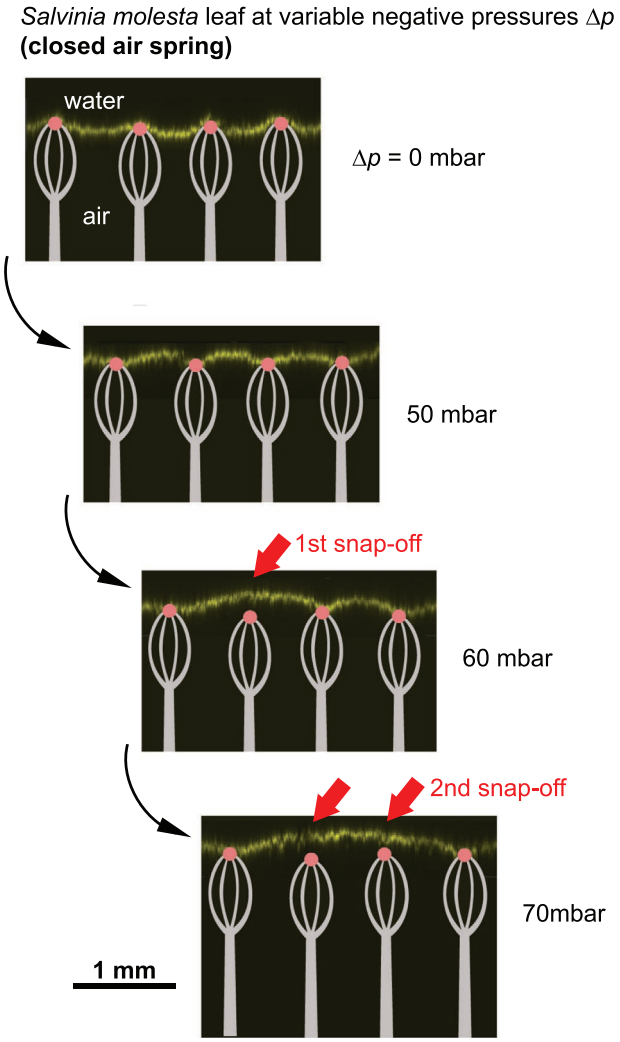

Figure 3. LSCM of the air–water interface—and the direct observation of snap-off processes at underpressure: When exposed to an increasing underpressure, the trapped air of a submerged half-leaf of *Salvinia molesta* expands and the air–water interface between the adhesive hair tips is bent more and more as could be observed using laser confocal microscopy. The hairs with adhesive (hydrophilic) pinning sites (red) are schematically drawn. Here at about 60 mbar underpressure, the first snap-off occurred, followed by a further one at 70 mbar. The first snap-off occurred at an underpressure of ≈55–60 mbar ($n = 50$).

2.3. A Suggested Model for Explaining the Remaining Factor of 100 in Air Retention Stability

A simple model may help to explain the nature of the missing part of the air-retaining force at underpressures (and in fact also at overpressures). As the hydrophilic pins at the end of the hairs lead to an entrapment of the air layer, underpressure leads to an expansion of the air layer—while the entrapped amount of air and the temperature remain the same. Such an expansion of the volume of the entrapped gas at underpressure is achieved by two effects: 1) the elastic properties of the crown of the egg-beater-shaped hairs allow elongation at underpressure and 2) the deformation of the meniscus at underpressure. As we had shown above in the LSCM experiments the deformation of the meniscus at underpressure also allows for volume expansion even for the case of stiff hairs. Volume expansion of a gas at constant temperature leads to a decrease of pressure. For ideal gases—which is a particularly good approximation for air at ambient conditions and even at slightly elevated pressures—the universal gas equation is valid

$$p \cdot V = n \cdot R \cdot T \tag{1}$$

where p denotes the gas pressure, V the gas volume, n the amount of substance in units of mol, R the universal gas constant, and T denotes the absolute temperature. An expansion of the gas volume due to underpressure thus creates a decrease in pressure of the gas volume and this, in turn, creates a restoring force pulling the water interface toward the leaf. In this model, the entrapped gas volume acts as a pneumatic spring or air spring. This shows a brilliant and at the same time simple strategy of the plant: It "delegates" about 99% of the overall restoring force, needed to keep the air to the entrapped air volume, which acts as an elastic "air cushion."

The key remaining question is whether this force is really the relevant force for explaining the observed increase by a factor of 100 in air layer stability at underpressure.

To answer this question, we designed the following experiment: We expose a living leaf of *Salvinia molesta* to different underpressures in two situations—one with the restoring force of the entrapped air switched on and one with the restoring force of the entrapped air switched off. The latter is achieved simply by opening the air cushion and directly connecting it with the ambient air (**Figure 4**d). In this way, there is no entrapped air volume and the pressure in the air layer is always adapting itself to the outside pressure.

2.4. Quantitative Evaluation of the Effect of the Experimentally Observed Meniscus Deformation on the Air-Spring Effect

To estimate the effect of the air spring more precisely, we considered the effect of the applied negative pressure on the air–water interface, as measured by confocal microscopy and shown in Figure 3. With an applied negative pressure of 60 mbar, the interface moved from 120 µm inwardly convex at 0 mbar to ≈120 µm outwardly convex. In order to calculate the absolute air volume change per area, we have taken a closer look at the leaf surface and estimated the local distribution of pinning points. This degree of bulging of 120 µm was observed between two pinning points with a distance of about 800 µm. The air–water interface between closer fitting pinning points was less bulged because an interface with constant curvature was formed.

The upper part in **Figure 5** shows a view of half a leaf. The density of trichomes and thus the pinning points varies slightly within the leaf, with a particularly low density always being found toward the middle of the leaf, closer to the stem (left side in this example). This is exactly where the first loss of contact usually occurs due to the particularly large distances of pinning sites. Due to the disordered distribution of the contact points, a volume calculation of the air under the deformed interface is only possible using an empirical model of the topography.

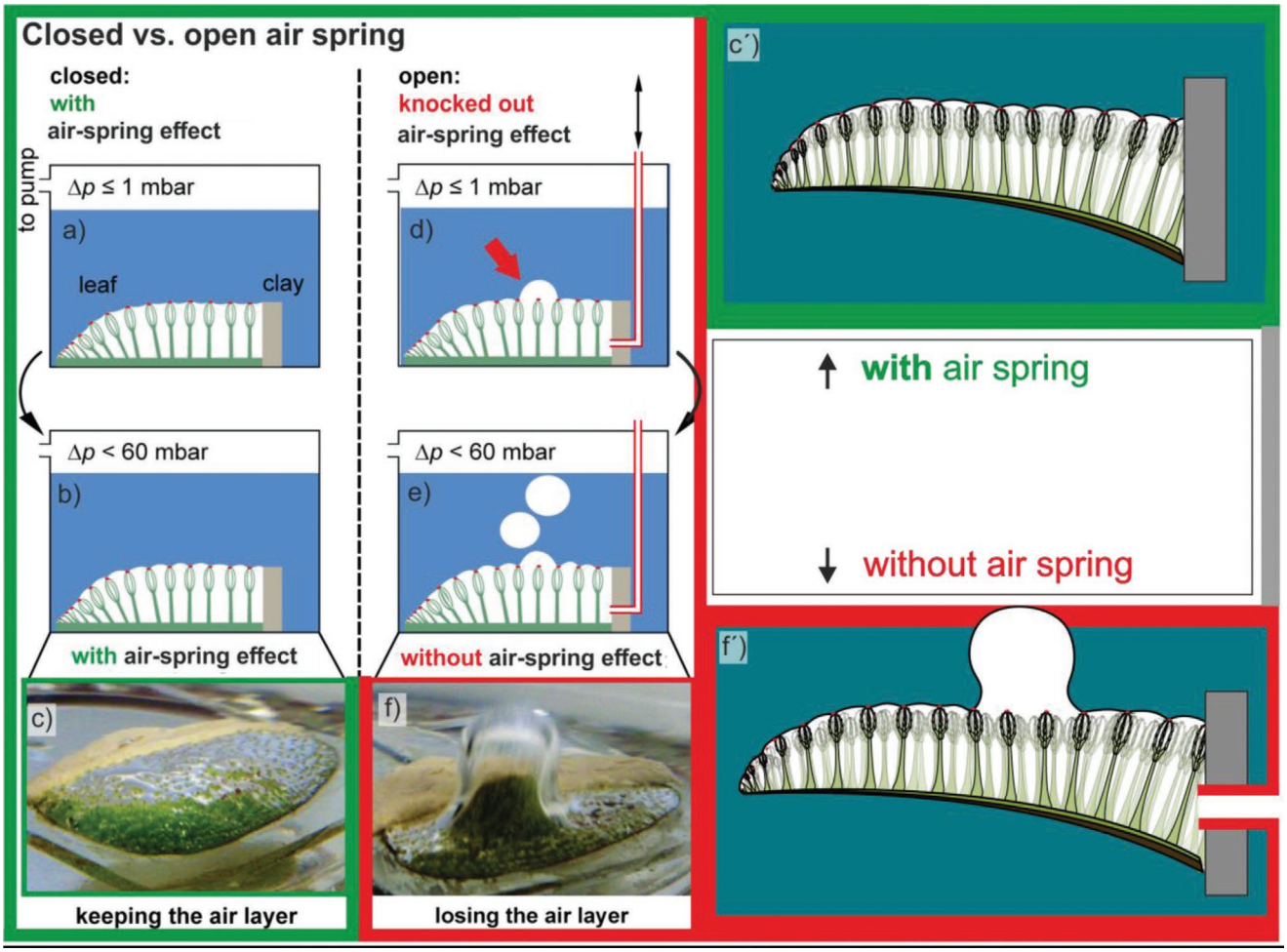

Figure 4. *Salvinia molesta* leaves with (left) and without ("knocked out") (right) air-spring effect: We mounted half of a leaf onto a glass plate and sealed it at the middle section. d) The underpressure needed for the first snap-off drastically decreased from 60 mbar to less than 1 mbar if the volume of the trapped air was connected to the atmosphere by a tube. e,f) If higher underpressure is applied to the open leaf, a steam of ascending air bubbles can be observed. This situation simulates an infinitely thick air layer, or an ultra-soft air spring. The value of 1 mbar is exactly the value we expect, when only considering the measured water adhesion force of the hydrophilic tips of the hairs as stabilizing force acting at the air–water interface. A high persistence of the air layer against underpressure therefore needs both: hydrophilic tips and a stiff air spring, meaning a thinnest possible air layer.

Figure 5a shows a possible scenario that corresponds to the situation in Figure 4c. In the situation, the volume of air under the bulged part of the air cushion is about 60% of a flat air layer of the same height. In our model, we assumed that all contact points were situated in one plane 120 µm below the highest elevation. With these figures, we could estimate the expansion of the volume. The volume of air under the upwardly bulging interface was about $0.072 \times 1 \times 1$ mm^3 at a maximum height of 120 µm. If we take into account the initially inwardly bulging boundary surface with also $0.072 \times 1 \times 1$ mm^3, we get $0.144 \times 1 \times 1$ mm^3. Since the trichomes expand according to their spring constant (of 2.1 N m^{-1}) due to the outward curvature of the boundary surface, another 0.01 mm^3 is added here at 19 µN.[17,55] This elongation is applied twice, since the trichomes are first compressed and then stretched. This results in a total of 0.02 mm^3 additional volume.

This means that ≈85% of the volume change of the entrapped gas can be attributed to the deformation of the water meniscus due to pressure change and the elasticity of the eggbeater basket contributes to the volume change by only 15% (as compared to the bulging of the interface).

It is of interest to study the influence of the Laplace pressure, which reduces the internal pressure of the leaf. Assuming a distance of 800 µm between two pinning points and a height of the segment of 120 µm, the radius of curvature of the air–water interface is ≈725 µm. We can now calculate the Laplace pressure:

$$\Delta p = \frac{2 \cdot \gamma}{R} \tag{2}$$

with γ being the surface tension of water (72 mN m^{-1}) and R being the radius of curvature of the water meniscus. This results in a Laplace pressure of about 2 mbar using a simplified spherical cap geometry. We can neglect this pressure contribution for two reasons: i) it is low in comparison to the 60 mbar external pressure and ii) it acts first outward (before underpressure application) and then inward (after application

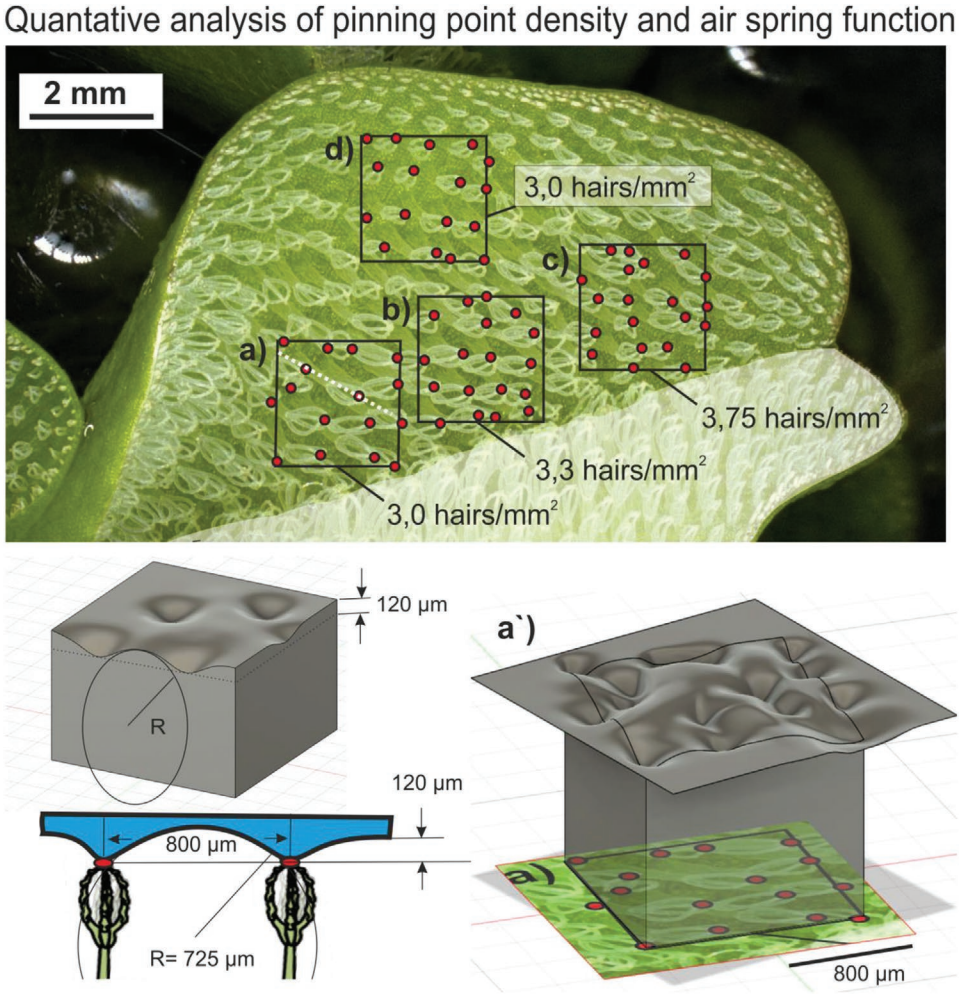

Figure 5. The areal density of pinning points varies over the leaf's surface roughly between 3.0 and 3.75 hairs mm^{-2}. a) The lowest density is realized in the central region closer to the leaf stem. With negative pressure applied, the air/water interface is most dented in this region. This is the position the first snap-off will take place. From in situ confocal microscopy images of similar leaves we know that the amplitude of corrugation is about 120 µm at 60 mbar underpressure. Using these values, a´) we can calculate a model profile which shows 60% volume fraction of air in the corrugated upper zone. With these data we can determine the effective air cushion thickness (air spring) to be 2.73 mm for this type of adult (half) leaf of *Salvinia molesta*.

of the underpressure). Due to the pressure change, the volume of air in the leaf increases by ≈0.164 mm^3 per mm^2 (164 µm increase in height). To achieve this increase in height, we have applied a negative pressure of 60 mbar, i.e., we have reduced the initial pressure by 6%. This means that the air cushion of the leaf works as an air spring with a height of 164 µm/6% = 2.73 mm. This calculated value of the effective height of the air (spring) layer of a *Salvinia molesta* leaf is in remarkably good agreement with the actually observed length of the trichomes.

2.5. Experimental Proof of the Air-Spring Model: Air Layer Stability of a Submerged Leaf of *Salvinia molesta* with Knocked Out Air-Spring Effect

To prove the function of the air spring, we prepared *Salvinia molesta* leaves with knocked out thin layer air-spring effect, i.e., with an air layer of unlimited thickness, which means an open air volume (infinitely soft air spring). Experimentally, we realized this by the following method. We mounted half of a leaf onto a glass plate and sealed it at the middle section. Then we build in a tube connecting the trapped air volume of the leaf with the outside atmosphere. Consequently, an infinite air film thickness was simulated equivalent with an infinite soft air spring. Now, only the water adhesion forces of the hair tips should be responsible for the remaining underpressure resistance. The first snap-off now occurred at (0.79 ± 0.22) mbar underpressure (n = 20). At higher underpressures, air bubbles started forming through the open leaves leading to an ascending chain of bubbles (Figure 4). Thus, within the limits of experimental accuracy, we could exactly reproduce the calculated underpressure value. The air layer of a leaf can persist 0.6 mbar, provided that only the water adhesion force of the hydrophilic hair tips is considered. This shows that the effect of a sufficiently thin layer air spring (hard spring) in combination with the flexibility of the hairs is the crucial component in explaining the *Salvinia* effect.

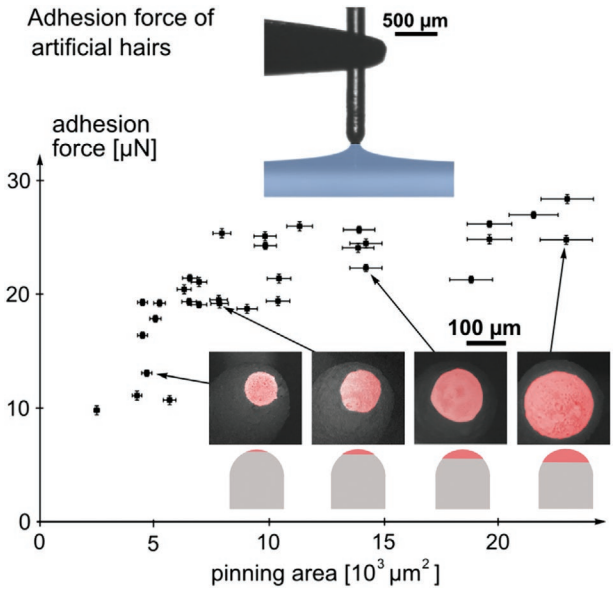

Figure 6. Artificial hairs with varying adhesive spot size: Like their biological model—the hairs of *Salvinia molesta*—the artificial (superhydrophobic) hairs were equipped with hydrophilically modified pinning areas (red colored in the SEM image). With increasing pinning area, we observe a strongly growing water adhesion force to 20 µN up to a pinning area of about 100 µm in diameter, followed by only a slight increase up to 25 µN with further rising pinning area.

2.6. Artificial Hairs with Varying Adhesive Spot Size

While the pinning effect of the ends of the trichomes alone is not sufficient to explain the restoring forces against air loss at underpressure, it provides the basis for entrapping a finite volume of air, which, in turn, is able to act as an air spring. To understand this pinning effect of the hydrophilic tips of the *Salvinia* trichomes and its dependence on the size and diameter of the hydrophilic pinning areas in more detail, we designed base elements of artificial *Salvinia* effect surfaces (epoxy pillars with a round top) artificially which were equipped with a micro-structured superhydrophobic coating as described in the Experimental Section (see **Figure 6**). The tips of the pillars were hydrophilically functionalized as its biological role model, the hairs of *Salvinia molesta*. We calculated the water adhesion force using the presented meniscus technique depending on the hydrophilic pinning area, which we determined by scanning electron microscopy (SEM). The results are shown in Figure 5. The water adhesion force rises to values of about 20 µN with increasing pinning area and stabilizes at this level (at about 10×10^3 µm²). From then on, it only rises slightly with further increasing pinning area to about 25 µN when the round pillar tip is almost fully hydrophilically coated. So, for the design of artificial *Salvinia* effect surfaces, it is important that the hydrophilic pinning area exceeds roughly the value mentioned above to get high water adhesion forces and thus high air layer persistence. The results indicate that in this geometry, larger pinning areas are not yielding higher forces. However, in technological applications, e.g., in ship hulls, they might have a detrimental effect on friction reduction.

The cross-section of the hydrophilic surface of *Salvinia molesta*, at 50 µm, is significantly larger than the minimum area found here, where maximum adhesive force is already achieved. This indicates that the hydrophilicity is not as pronounced in the biological model. In fact, our preliminary investigations on artificial and natural trichomes coated with different reference materials with different contact angles showed that the contact angle of the hydrophilic spots in the natural model is about 35° and not 20° as in the case of poly-(2-vinylpyridine) used here. This means that nature seems to compensate the lower hydrophilicity with a larger area of the hydrophilic area.

2.7. Reaction of the Immersed *Salvinia* Leaf at Overpressure with and without Air-Spring Effect

After we have seen what dramatic effect the loss of the air spring has on the stability in the case of underpressure (negative pressure), it is of interest to observe what the contribution of the air spring at overpressure (positive pressure) is. This is highly relevant both in the case of pressure fluctuations (which include positive and negative pressures), and at higher water depths, where the gravitational pressure load acts as at overpressure. To study the behavior of the leaf at overpressure and to quantify the air loss, we mounted a complete leaf on a glass carrier and immersed it in an acrylic cylinder under water. Even after 1 week under water at a depth of 40 cm, no air loss was detectable, at least visually. Only at higher water depths of, e.g., 2 m, a decrease of air was observed within a few days.

The situation is completely different when the air volume of the submerged leaf is in contact with the atmosphere by short-cutting the sealed air volume of the leaf directly to the ambient pressure. We stitched a thin cannula into this sealed air volume, the plastron, of the leaf submerged at a depth of 38 cm beneath the water surface, which was connected by a capillary to a vessel at the level of the water surface (see **Figure 7**a). When the valve in Figure 7a was opened, the air flowed evaded from the plant leave into the vessel at water level and thus spontaneously emptied the air cushion held by the leaf, proving that the dewetting forces of the hydrophobic hairs alone are not able to keep the air even at a depth of only 38 cm.

For a quantitative analysis of this process, a diving bell collected the air displaced by the water pressure, which exited the capillary in the form of bubbles. The video-supported, time-resolved counting of the bubbles at the end of the 1 mm diameter capillary and the measurement of the total volume by means of a precision syringe allowed a quantitative analysis of the deflation of the leaf as a function of time (Figure 7f). The volume versus time curve shows two different dynamic regimes: a rapid deflation of the air of the leaf through the dry capillary, followed by a slower depletion, which can be explained by the fact that finally water enters the capillary and continues to displace the remaining air from the capillary. The process comes to a standstill when the last bubble (in the experiment shown as bubble no. 10) detaches from the capillary. A complete relaxation of the system is not expected due to the capillary pressure of about 2.88 mbar due to the radius of the last remaining bubble at the end of the capillary ($2\,\sigma/r = 2 \times 72$ mN m^{-1}/0.5 mm). If this residual pressure is taken into account, ≈100 µL (=351 mm of the 38 cm

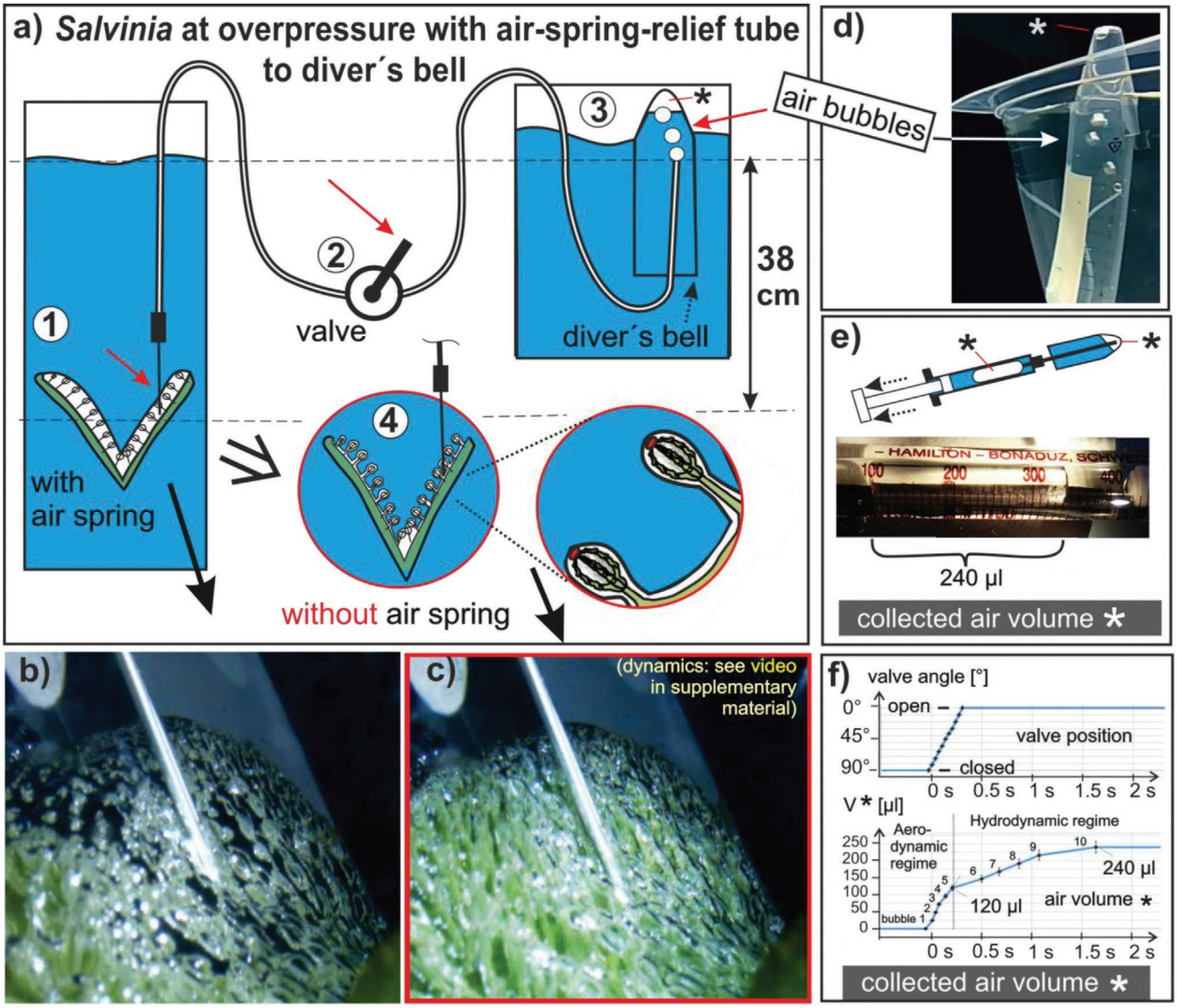

Figure 7. *Salvinia molesta* leaves b) with and c) without ("knocked out") air-spring effect: a), 1) we mounted a complete leaf on a glass plate and immersed it 38 cm under water. 3) A capillary connected the air volume with a higher placed vessel, but first 2) with the valve closed. When the valve was opened, the air immediately flowed upward, leaving a much emptier leaf at depth. e) A diver's bell collected the extracted air which could finally be measured using a precision syringe. A quantitative analysis of the video, which can be seen as Supporting Information shows that within the first 0.5 s air with about 38% of the air-retaining volume of the leaf is drained into the diver's bell until presumably water enters the capillary, which slows down the appearance of air bubbles (hydrodynamic regime in (f)). The immediate collapse of the air layer when the air spring is switched off shows that the air spring is an enormously important aid for the plant, not only when there is negative pressure (Figure 4), but also when there is excess pressure.

underwater tube length x π x (300 µm)^2) of the air should come from the displacement process of the rising water. This means only 140 µL come from the leaf, which, after microscopic analysis of the plant leaf being used and 3D modeling, provides a total of 380 µL of entrapped air volume in the plant leaf (see **Figure 8**). Thus, the air loss of the leaf corresponds to a volume of ≈37% of the entire air envelope volume spanned by the trichomes as soon as the valve is opened (aerodynamic regime in Figure 7f). Then water enters the tube and subsequently displaces the air from the tube at a slower speed (hydrodynamic regime in Figure 7f). Our experiments showed that the process of deflating and inflating the leaf can be repeated several times, if only a part of the 140 µL are allowed to escape (not shown in Figure 7).

3. Conclusions

By immersing *Salvinia molesta* leaves under water and exposing them to an underpressure, we find an impressive stability against air bubble formation up to a value of about 60 mbar, which is almost 100 times higher than what has been expected from our water adhesion force measurements: With a hair density of about three pinning points per mm^2, the water adhesion force of about 20 µN leads to a value of only about 0.6 mbar for the underpressure resistance.

During experiments with leaves with knocked-out air-spring effect, in which the trapped air volume of the leaves was connected to the atmosphere, representing an infinite air reservoir

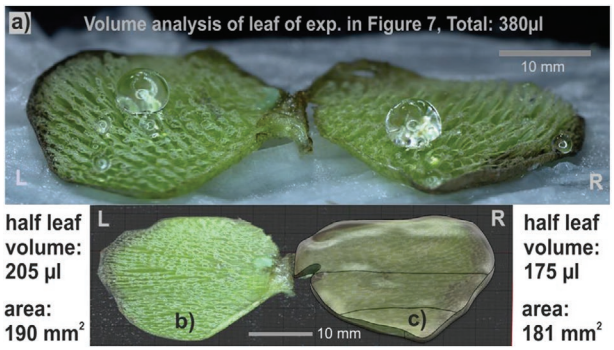

Figure 8. a) To calculate the volume of the leaf from Figure 7d, it was divided into two halves after the overpressure experiment. By microscopic measurement, a 3D model of the trichome envelope of the leaf was made (shown for the right half in (c) in gray shading), and thus the volume was determined: the right half-leaf, including the trichomes themselves, has a potential air-holding volume of about 175 µL, the left half-leaf has 205 µL, corresponding to a total volume of the entrapped air layer of the leaf of 380 µL.

with no air entrapment, we measured the corresponding weak underpressure resistance: At about 0.6 mbar, the first pinning point of the air–water interface was lost. At higher underpressures, a stream of air bubbles ascended from the leaf surface and the air layer was lost.

The impressive stability of the closed leaf system, which was also confirmed by in situ laser confocal microscopy, mainly results from the air-spring effect of an entrapped air volume. The air layer on the leaf requires a force to be expanded or compressed and serves as a spring that significantly reduces the movement of the air/water interface for a given underpressure. The shape of the resulting expanded air cushion is determined by the interaction of surface tension and the flexibility of the hairs. Only when a critical volume of the air layer is exceeded, the first contact points are lose, because the outward bended air/water interface pulls too strongly (>20 µN) on the pinning sites at the end of the hairs.

Finally, artificial hairs with a varying hydrophilic pinning area showed similar adhesion forces (20 µN) as the natural model *Salvinia molesta* at an area of about 100 × 100 µm². In our experiments, larger pinning areas did not yield significantly higher adhesion forces.

The overpressure experiment, which is shown in Figure 7 (and in the video in the Supporting Information), proves the air spring is a very important protection against air loss not only at underpressure but also at overpressure.

To conclude, with the effect of the air layer as an elastic spring, a key factor for understanding the air-retaining properties of *Salvinia molesta* at fluctuating pressures was identified and quantitatively understood. The results may pave the way for designing air-retaining surfaces for technological applications such as drag reducing ship hulls, where the stability of the lubricating air layer at turbulent conditions and fluctuating pressures is a key requirement.

4. Experimental Section

Single Hair Adhesion Force Measurement: A single *Salvinia molesta* hair or an artificial hair was picked at its base with a tweezer which was fixed on a stepping motor with the hair tip downward.[56] The hair tip was then attached to the surface of a water-filled container standing below and removed from the surface with a velocity of 120 µm s^{-1}. When the tensile force caused by the increasing meniscus exceeded the water adhesion force to the hair tip, the meniscus snapped off. This process was captured with a CCD camera. The meniscus profile shortly before snap-off was now fitted with an elliptic function

$$y_{(x)} = -\frac{b}{a}\sqrt{a^2 - \left(x - a - \frac{c}{2}\right)^2} + b \tag{3}$$

with parameters a, b, and c as shown in Figure 2. Rotating $y(x)$ around the y-axis led to the lateral surface A of the water meniscus. The energy W needed to build the meniscus was the surface energy of the meniscus plus the surface energy of the contact area minus the surface energy of the original, unperturbed air–water interface

$$W = A \cdot \sigma + \pi\left(\frac{c}{2}\right)^2 \cdot \sigma' - \pi\left(a + \frac{c}{2}\right)^2 \cdot \sigma \tag{4}$$

with the water surface tension σ and the tension σ' of the interface between hair tip and water, which was unknown, but not necessary to know for the further calculation. The corresponding force pulling at the hair was then

$$F = \frac{\partial W}{\partial b} = \frac{\partial A}{\partial b} \cdot \sigma \tag{5}$$

which was equal to the water adhesion force of the hair tip.

Air–Water Interface Imaging at Variable Underpressures with Laser Confocal Microscopy: For imaging the air–water interface of a submerged *Salvinia molesta* leaf at variable underpressures, a self-made pressure cell with an optical window and a sample manipulator was used. The leaves were cut into half along the leaf axis in order to get a flat sample. The cutting edge was sealed using hydrophobic modeling clay. After filling the pressure cell with water, a sonicated aqueous suspension of fluorescent pigment PS10 (radiant color) was injected. The insoluble pigment particles sedimented onto the air–water interface within 20 min. After that, the opening of the cell was connected to a vacuum pump and a 10 L buffer recipient to apply variable underpressures. The fluorescent signal of the decorated air–water interface was imaged using a confocal laser scanning microscope (Leica TCS SP 2 X-1) system with an excitation wavelength of 458 and 488 nm and HC PL Fluotar 5x/0.15 POL Leica 5x dry objective.

Volume Calculations and Density of Pinning Points in Natural Leaves: The image of the leaf in Figure 4 was taken with a Keyence 3D microscope. The validated areas for the hair density calculations were approximately in one plain with a resolution of about 100 µm. For volume calculation of the air below the air/water interface with the software *fusion 360* (Autodesk), a surface of approximate constant curvature was manually modeled, using the lateral pinning point positions of the real leaf. The air volume was calculated by subtracting the volume of a box with the same height.

Air Layer Underpressure Stability Measurement: To measure the air layer stability of a submerged *Salvinia molesta* leaf, it was divided along the leaf axis into two parts, as it was done for the confocal imaging experiments. One of these half leaves was fixed onto a glass plate and sealed at the cutting edge using modeling clay. It was then put in a glass bottle filled with water up to a level of a few centimeters. The lid of the bottle was connected to a vacuum pump and a 10 L buffer recipient to apply variable underpressures. In case of the open leaf system, the as prepared leaf part was pierced through the piece of clay with a tube at the sealed side, which was connected to the atmosphere outside the bottle.

Preparation of Artificial Salvinia-Effect Hairs: The artificial hairs whose water adhesion force was measured in this work were epoxy pillars with a diameter of 220 µm and a round top. They were equipped with a micro-particle-filled Teflon AF coating (DuPont) with a water contact angle of (160.22 ± 0.54)° and a contact angle hysteresis of (3.74 ± 0.73)°,

both measured on flat surfaces. The tips were hydrophilized using poly-(2-vinylpyridine) (Polymer Standards Service) with a contact angle of (20.11 ± 0.28)°. The hairs were dipped into a thin film of polymer solution 3% in ethanol. After measuring the adhesion force using the capillary adhesion technique, each individual hair was examined with SEM to validate its adhesive surface area.

Overpressure Experiments: For the overpressure experiments, complete adult leaves of *Salvinia molesta* were glued with one side on a microscope slide with dental silicone (PRESIDENT COLTENE/Light body ref 60019949). Then a hydrophobized cannula was carefully mounted as close as possible to the base of the trichomes (cannula: 4 mm × 25 (blunt) B. Braun AG Germany, hydrophobization: Mecasurf MT1 solution, SURFACTIS Technol. Angres France) 10:1 w/w mixed with HMFS Partrices. The cannula was connected with the air-spring relief tube (2.2 m long polytetrafluoroethylene, 0.6 mm × 1 mm (inner and outer diameter) LHG Laborhandelsgesellschaft Germany). The air-spring relief valve was a 6 mm ball valve (Festo, Esslingen, Germany). As a diver's bell a 15 mL polypropylene centrifuge tube Carl Roth GmBH Karlsruhe, Germany, was used. The precision syringe was a model "Hamilton Gastight # 1750," Hamilton, Bonaduz Switzerland.

Supporting Information

Supporting Information is available from the Wiley Online Library or from the author.

Acknowledgements

The authors acknowledge financial support by the German Ministry of Education and Research, BMBF within the VIP Project ARES (Air REtaining Surfaces, 03V0751) and previously by the BIONA project, as well as support by the Baden-Wuerttemberg Stiftung and by the European Commission (EC) within the H2020-project AIRCOAT (Air Induced friction Reducing ship COATing). The AIRCOAT project has received funding from the European Union's Horizon 2020 research and innovation programme under grant agreement N° 764553. D.G. acknowledges support by the State of Baden-Wuerttemberg within a Baden-Wuerttemberg Scholarship. The authors thank Silas Walheim for his help with graphic arts and videos. The authors also acknowledge the earlier contributions of and discussions with members of their research groups in Karlsruhe at KIT (Aaron Kobler, Anke Kaltenmeier, Matthias Mail, Matthias Barczewski, Roland Gröger) and at the University of Bonn (Matthias Mayser, Matthias Mail).

Open access funding enabled and organized by Projekt DEAL.

Conflict of Interest

The authors declare no conflict of interest.

Keywords

air spring, biomimetics, *Salvinia* effect, super-hydrophobicity, underwater air retention

Received: June 3, 2020
Revised: August 3, 2020
Published online: September 29, 2020

[1] W. Barthlott, T. Schimmel, S. Wiersch, K. Koch, M. Brede, M. Barczewski, S. Walheim, A. Weis, A. Kaltenmaier, A. Leder, H. F. Bohn, *Adv. Mater.* **2010**, *22*, 2325.
[2] W. Barthlott, M. Mail, B. Bhushan, K. Koch, *Nano-Micro Lett.* **2017**, *9*, 23.
[3] B. Bhushan, Y. C. Jung, *Prog. Mater. Sci.* **2011**, *56*, 1.
[4] Y. C. Jung, B. Bhushan, *J. Phys.: Condens. Matter* **2010**, *22*, 035104.
[5] J. Busch, W. Barthlott, M. Brede, W. Terlau, M. Mail, *Philos. Trans. R. Soc., A* **2019**, *377*, 20180263.
[6] B. Bhushan, *Biomimetics - Bioinspired Hierarchical-Structured Surfaces for Green Science and Technology*, 3rd ed., Springer, New York **2018**.
[7] W. Barthlott, C. Neinhuis, *Planta* **1997**, *202*, 1.
[8] C. Neinhuis, W. Barthlott, *Ann. Bot.* **1997**, *79*, 667.
[9] R. Blossey, *Nat. Mater.* **2003**, *2*, 301.
[10] M. Callies, D. Quere, *Soft Matter* **2005**, *1*, 55.
[11] P. Roach, N. J. Shirtcliffe, M. I. Newton, *Soft Matter* **2008**, *4*, 224.
[12] W. Barthlott, M. D. Rafiqpoor, W. R. Erdelen, in *Biomimetic Research for Architecture and Building Construction* (Eds: J. Knippers, K. G. Nickel, T. Speck), Vol. *8*, Springer, Cham **2016**, pp. 11–55.
[13] W. Barthlott, M. Mail, C. Neinhuis, *Philos. Trans. R. Soc., A* **2016**, *374*, 20160191.
[14] Y. Y. Yan, N. Gao, W. Barthlott, *Adv. Colloid Interface Sci.* **2011**, *169*, 80.
[15] Y. H. Sun, Z. G. Guo, *Nanoscale Horiz.* **2019**, *4*, 52.
[16] Y. F. Si, Z. C. Dong, L. Jiang, *ACS Cent. Sci.* **2018**, *4*, 1102.
[17] M. Mail, A. Klein, H. Bleckmann, A. Schmitz, T. Scherer, P. T. Ruhr, G. Lovric, R. Frohlingsdorf, S. N. Gorb, W. Barthlott, *Beilstein J. Nanotechnol.* **2018**, *9*, 3039.
[18] J. Ou, B. Perot, J. P. Rothstein, *Phys. Fluids* **2004**, *16*, 4635.
[19] G. McHale, N. J. Shirtcliffe, C. R. Evans, M. I. Newton, *Appl. Phys. Lett.* **2009**, *94*, 064104.
[20] A. K. Balasubramanian, A. C. Miller, O. K. Rediniotis, *AIAA J.* **2004**, *42*, 411.
[21] N. J. Shirtcliffe, G. McHale, M. I. Newton, Y. Zhang, *ACS Appl. Mater. Interfaces* **2009**, *1*, 1316.
[22] G. McHale, M. I. Newton, N. J. Shirtcliffe, *Soft Matter* **2010**, *6*, 714.
[23] H. Y. Dong, M. J. Cheng, Y. J. Zhang, H. Wei, F. Shi, *J. Mater. Chem. A* **2013**, *1*, 5886.
[24] W. T. Rong, H. F. Zhang, Z. G. Mao, X. W. Liu, K. G. Song, *Mater. Res. Express* **2020**, *7*, 11.
[25] C. H. Choi, C. J. Kim, *Phys. Rev. Lett.* **2006**, *96*, 066001.
[26] C. Lee, C. H. Choi, C. J. Kim, *Phys. Rev. Lett.* **2008**, *101*, 064501.
[27] F. Feuillebois, M. Z. Bazant, O. I. Vinogradova, *Phys. Rev. Lett.* **2009**, *102*, 026001.
[28] K. Koch, H. F. Bohn, W. Barthlott, *Langmuir* **2009**, *25*, 14116.
[29] B. Bhushan, *Beilstein J. Nanotechnol.* **2011**, *2*, 66.
[30] A. Solga, Z. Cerman, B. F. Striffler, M. Spaeth, W. Barthlott, *Bioinspiration Biomimetics* **2007**, *2*, S126.
[31] X. L. Sheng, J. H. Zhang, *Colloids Surf., A* **2011**, *377*, 374.
[32] M. A. Samaha, H. V. Tafreshi, M. Gad-el-Hak, *C. R. Mec.* **2012**, *340*, 18.
[33] J. Hunt, B. Bhushan, *J. Colloid Interface Sci.* **2011**, *363*, 187.
[34] C. Lee, C. J. Kim, *Langmuir* **2009**, *25*, 12812.
[35] W. Konrad, C. Apeltauer, J. Frauendiener, W. Barthlott, A. Roth-Nebelsick, *J. Bionic Eng.* **2009**, *6*, 350.
[36] M. C. Xu, G. U. Sun, C. J. Kim, *Phys. Rev. Lett.* **2014**, *113*, 136103.
[37] M. Xu, G. Sun, C. C. Kim, in *2014 IEEE 27th Int. Conf. on Micro Electro Mechanical Systems (MEMS)*, IEEE, Piscataway, NJ **2014**, pp. 668–671.
[38] R. Poetes, K. Holtzmann, K. Franze, U. Steiner, *Phys. Rev. Lett.* **2010**, *105*, 166104.
[39] Y. W. Zheng, X. Zhou, Z. Q. Xing, T. M. Tu, *RSC Adv.* **2018**, *8*, 10719.
[40] W. Barthlott, M. Mail, B. Bhushan, K. Koch, *Nano-Micro Lett.* **2017**, *9*, 23.
[41] M. J. Mayser, H. F. Bohn, M. Reker, W. Barthlott, *Beilstein J. Nanotechnol.* **2014**, *5*, 812.
[42] M. Moosmann, T.h. Schimmel, W. Barthlott, M. Mail, *Beilstein J. Nanotechnol.* **2017**, *8*, 1671.
[43] O. Tricinci, T. Terencio, B. Mazzolai, N. M. Pugno, F. Greco, V. Mattoli, *ACS Appl. Mater. Interfaces* **2015**, *7*, 25560.

[44] O. Tricinci, T. Terencio, N. M. Pugno, F. Greco, B. Mazzolai, V. Mattoli, *Micromachines* **2017**, *8*, 366.
[45] Y. Xiang, S. Huang, T. Y. Huang, A. Dong, D. Cao, H. Li, Y. Xue, P. Lv, H. Duan, *Proc. Natl. Acad. Sci. U. S. A.* **2020**, *117*, 2282.
[46] C. Y. Yang, C. Y. Yang, C. K. Sung, *Jpn. J. Appl. Phys.* **2013**, *52*, 06GF08.
[47] M. Mail, M. Moosmann, P. Hager, W. Barthlott, *Philos. Trans. R. Soc., A* **2019**, *377*, 20190126.
[48] Y. W. Zheng, X. Zhou, Z. Q. Xing, T. M. Tu, *Text. Res. J.* **2019**, *89*, 2859.
[49] M. J. Mayser, W. Barthlott, *Integr. Comp. Biol.* **2014**, *54*, 1001.
[50] C. Zeiger, I. C. R. da Silva, M. Mail, M. N. Kavalenka, W. Barthlott, H. Holscher, *Bioinspiration Biomimetics* **2016**, *11*, 056003.
[51] Y. Yang, X. J. Li, X. Zheng, Z. Y. Chen, Q. F. Zhou, Y. Chen, *Adv. Mater.* **2018**, *30*, 1704912.
[52] W. Barthlott, M. Moosmann, I. Noll, M. Akdere, J. Wagner, N. Roling, L. Koepchen-Thoma, M. A. K. Azad, K. Klopp, T. Gries, M. Mail, *Philos. Trans. R. Soc., A* **2020**, *378*, 20190447.
[53] W. Barthlott, S. Wiersch, Z. Colic, K. Koch, *Botany* **2009**, *87*, 830.
[54] W. Barthlott, E. Wollenweber, in *Zur Feinstruktur, Chemie und taxonomischen Signifikanz epicuticularer Wachse und ähnlicher Sekrete* (Ed: W. Rauh), Vol. *32*, Akademie der Wissenschaften und der Literatur, Mainz, Franz Steiner GmbH Wiesbaden **1981**, p. 101.
[55] P. Ditsche, E. Gorb, M. Mayser, S. Gorb, T. Schimmel, W. Barthlott, *Appl. Phys. A: Mater. Sci. Process.* **2015**, *121*, 505.
[56] D. Gandyra, S. Walheim, S. Gorb, W. Barthlott, T. Schimmel, *Beilstein J. Nanotechnol.* **2015**, *6*, 11.
[57] M. Amabili, A. Giacomello, S. Meloni, C. M. Casciola, *Adv. Mater. Interfaces* **2015**, *2*, 1500248.
[58] K. Zhou, D. M. Li, P. H. Xue, P. Wang, Y. Zhao, M. H. Jin, *Colloids Surf., A* **2020**, *590*.
[59] M. Röhrig, M. Mail, M. Schneider, H. Louvin, A. Hopf, T.h. Schimmel, M. Worgull, H. Hölscher, *Adv. Mater. Interfaces* **2014**, *1*, 1300083.